Electronic supplementary information for

3D cell electrorotation and imaging for measuring multiple cellular biophysical properties

Liang Huang, Peng Zhao, Wenhui Wang*

State Key Laboratory of Precision Measurement Technology and Instrument, Department of Precision Instrument, Tsinghua University, Beijing, China 100084

**Corresponding author: wwh@tsinghua.edu.cn*

Selection criterion of the sidewall electrode geometry

The DEP force and torque are proportional to ∇E^2 and E^2 respectively, which are both related to the electrode shape. Fig. S1a-c shows three typical electrode geometric shapes (of round, squared and sharp tip) with the same microchannel width (200 μm). Fig. S1d is the simulated electric field strength (E_{rms}) distribution results of the three shapes in one period along the cutline *A-A*, when the four sidewall electrodes are applied with signals of $V_1=10\sin(\omega t)$, $V_2=10\sin(\omega t+\pi/2)$, $V_3=10\sin(\omega t+\pi)$, $V_4=10\sin(\omega t+3\pi/2)$, and the bottom electrode is floating. At the same AC signal amplitude (10 V), the sharp electrodes yield the greatest electric field strength, and thus greatest torque, which is favored for electric efficiency in rotation. The sharp electrodes also work best by generating the greatest DEP forces in single cell loading. Assuming $\varepsilon_m=100\varepsilon_0$, R=6 μm, and $\mathrm{Re}[K_{\mathrm{CM}}]=0.5$, we obtained from Equation 1 the DEP forces (Fig. S1e) along the cutline A-A in couple with the simulated ∇E^2 by setting electrodes 1, 2, and 5 floating, $V_2=10\sin(\omega t)$, $V_4=10\sin(\omega t+\pi)$. From the graph, sharp electrodes generate the greatest DEP force.

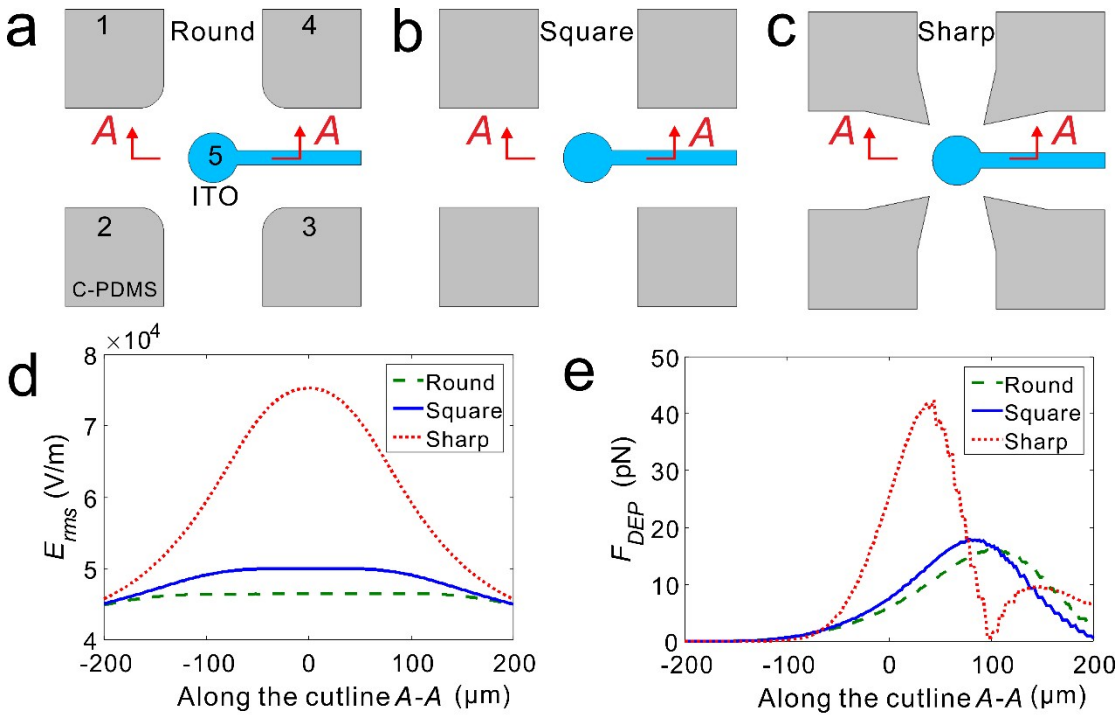

Fig. S1. Comparison of the electric field and DEP force for electrodes of different shape. **(a-c)** Top view of three typical electrode shapes. **(d)** The electric field strength along the cutline *A*-*A* (Vp-p=10 V). **(e)** DEP force distribution along the cutline *A*-*A* (Vp-p=10 V).

Validation of AC signals for producing rotating electric fields

When there is a rotating electric field, cells inside the electric field would rotate as well. So the key thing is to configure the AC signals on the electrodes such that a rotating electric field is induced. Fig. S2a-c show the AC signal configuration schemes for rotations about Z-axis (in-plane, top view), Y-axis (out-of-plane, side view *A*-*A*) and X-axis (out-of-plane, side view *B*-*B*). Fig. S2d-f are the simulation results of the electric field at four time beings in one period. For in-plane rotation about Z-axis, AC signals with equal amplitude but 90° phase shift are applied to the four sidewall electrodes, leaving the bottom electrode electrically floating. For out-of-plane rotation about Y- or X-axis, AC signals are applied to all the electrodes as shown in Fig. S2bc. Clearly, a rotating electric field is confirmed to incur about Z-, Y-, and X-axis respectively. Using the same simulation method, the direction of the rotating electric field can be validated as well.

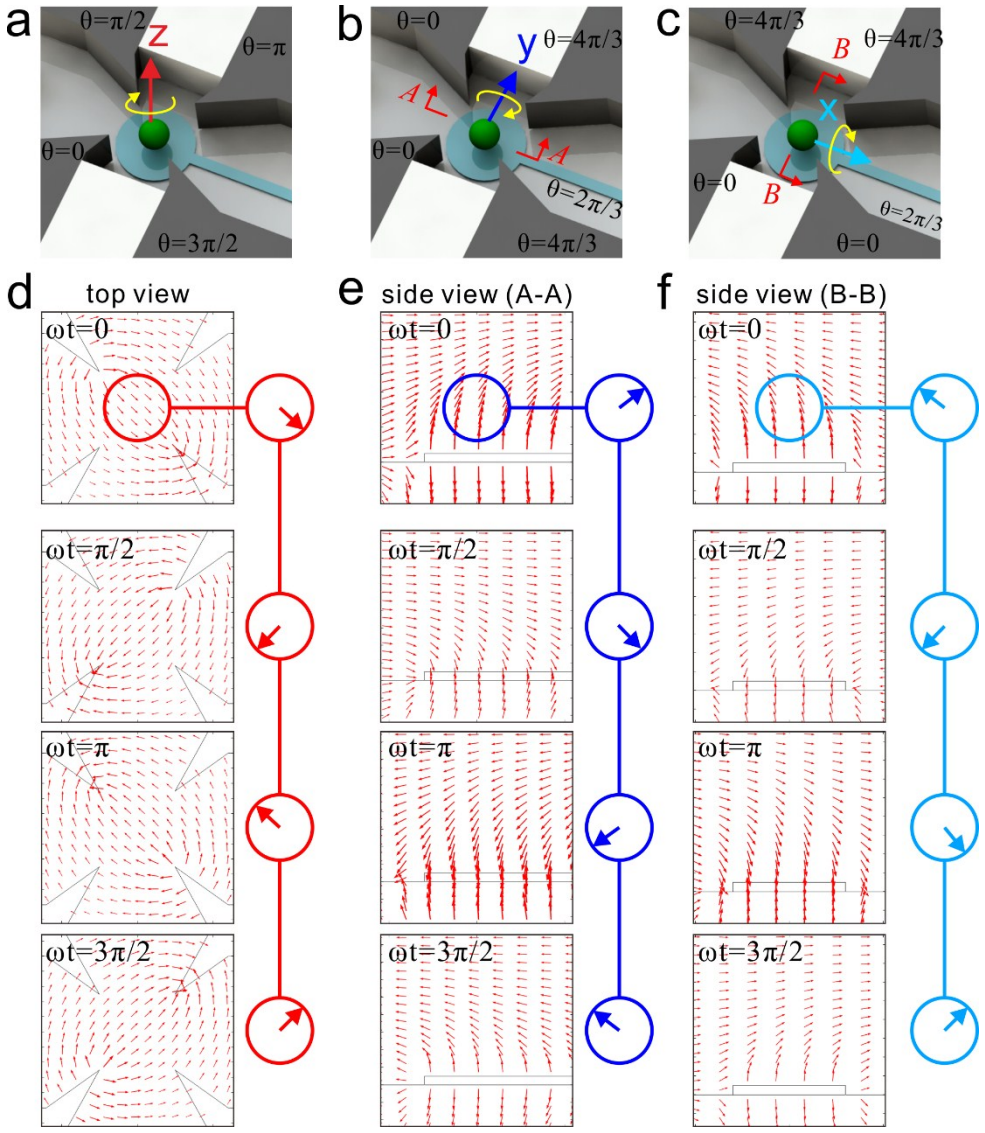

Fig. S2. The AC signal configuration schemes to induce rotating electric field about **(a)** Z-axis, **(b)** Y-axis and **(c)** X-axis. **(d-f)** The corresponding simulation results for the rotating electric field with its instantaneous direction labeled by arrows at four time beings in one period.

Optimization analysis of the phase shift for out-of-plane rotation

For out-of-plane rotation, a phase shift value of [30°, 170°] was found to be able to produce a workable rotating electric field on the vertical plane. Within this range, we can determine an optimal value for the phase shift by considering two factors, i) the mean of electric field strength over one AC signal period should be maximal for the highest electrical efficiency in cell rotation, 2) the standard deviation of electric field strength over one period should be minimal such that the rotation can be stable due to a uniform electric field. To quantify the two factors, we picked the rotation chamber center as the probing point in calculation, and set a phase shift interval of 10°. Fig. S3 shows the mean and standard deviation of electric field strength vs phase shift. The mean peaked at 110° and the standard deviation reached its lowest at 130°, thus finally we chose 120° for the phase

shift as a compromise.

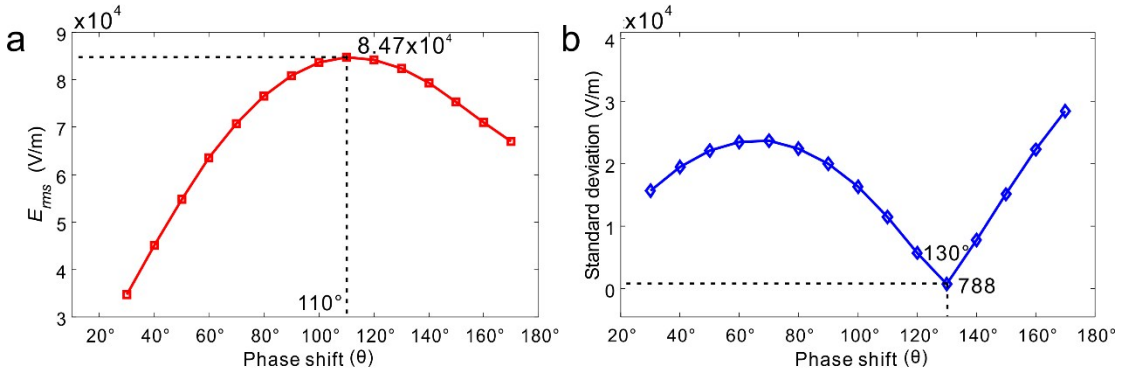

Fig. S3. The effect of phase shift on the rotating electric fields for out-of-plane rotation. **(a)** The mean of electric field strength vs phase shift. **(b)** The standard deviation of electric field strength vs phase shift.

The method for estimating the equilibrium position for the cell rotating in the gap of electrodes

When the cell rotates in the gap of electrodes, its free-body diagram is shown in Fig. S4a. Decoupling the rotation and translation, we simply take the equilibrium position as where the resultant forces in the horizontal and vertical directions are both zero.

Force equilibrium in the horizontal (X-axis) direction yields

$$F_{ITO} \cdot \sin\theta_1 = F_{C-PDMS} \cdot \sin\theta_2 . \tag{S1}$$

Substituting the DEP force F_{ITO} generated by ITO and $F_{C\text{-}PDMS}$ by C-PDMS electrodes, we have

$$2\pi R^3 \varepsilon_m Re[K_{CM}] \nabla E_{ITO}^2 \sin\theta_1 = 2\pi R^3 \varepsilon_m Re[K_{CM}] \nabla E_{CPDMS}^2 \sin\theta_2 . \tag{S2}$$

Simplifying Equation S2 we have

$$\nabla E_{ITO}^2 \cdot \vec{x} - \nabla E_{CPDMS}^2 \cdot \vec{x} = 0 . \tag{S3}$$

Considering the left-hand side is actually the X-component of ∇E^2, Equation S3 can be converted as

$$\nabla E^2 \cdot \vec{x} = 0 , \tag{S4}$$

where E is the resultant electric field of both electrodes.

Similarly, force equilibrium in the vertical (Z-axis) direction yields

$$F_{ITO} \cdot \cos\theta_1 + F_{C-PDMS} \cdot \cos\theta_2 + F_{buoyancy} = G , \tag{S5}$$

where G is the gravity, $F_{buoyancy}$ is the buoyancy force. Rewriting Equation S5 we get

$$\nabla E_{ITO}^2 \cdot \vec{z} + \nabla E_{C-PDMS}^2 \cdot \vec{z} = \frac{2(\rho_{cell} - \rho_{med})g}{3\varepsilon_m Re[K_{CM}]} , \tag{S6}$$

Considering the left-hand side is actually the Z-component of ∇E^2, Equation S6 can be converted as

$$\nabla E^2 \cdot \vec{z} = \frac{2(\rho_{cell} - \rho_{med})g}{3\varepsilon_m Re[K_{CM}]} \tag{S7}$$

We set that Vp-p=10 V, f=1 MHz, $Re[K_{CM}] = -0.06$, $\varepsilon_m = 60\varepsilon_0$, $\rho_{cell} = 1.077 \times 10^3 kg/m^3$, $\rho_{med} = 1.017 \times 10^3 kg/m^3$.

$$\nabla E^2 \cdot \vec{z} = 1.35 \times 10^{13} V^2/m^3 \tag{S8}$$

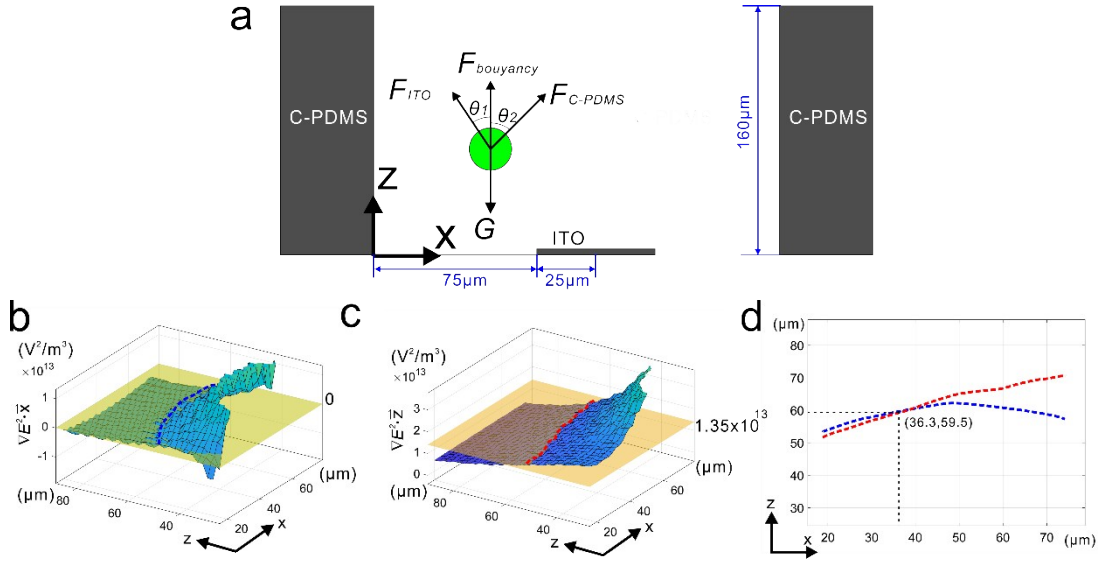

Fig. S4. Estimation of the equilibrium position for the cell rotating in the gap of electrodes. **(a)** The free-body diagram of the side-view cell (only considering forces). Simulation results when satisfying the equilibrium condition in the **(b)** horizontal direction and **(c)** vertical direction. **(d)** The equilibrium position when both conditions are met.

Using finite element analysis with commercially available software, Comsol 5.2b, we simulated and calculated the ∇E^2 components in both X- and Z-axis. Based on this, we plot the simulation results in Fig. S4bc that make Equations S4 and S8 hold. For the rotating case in Fig. 4i, the simulation results indicate that the cell would be balanced at (36.3 μm, 59.5 μm), which is in good agreement with the experimental results.

Micro-device fabrication procedure

Fig. S5 illustrates the fabrication procedure of the micro-device. A 160 μm-thick layer of negative photoresist (SU8-2075, MicroChem Corp.) was first spin-coated and photo patterned to obtain a channel mold. C-PDMS was then plastered on the mold with a blade to remove the excess conductive polymer. After being cured (80°C, 30 min), pure PDMS was poured on the mold and cured again. Finally, the PDMS/C-PDMS channel was unmolded and bonded to an ITO glass substrate with patterned electrodes

and V-shaped pillars (SU-8). The patterned electrodes on ITO glass were fabricated by photolithography with negative photoresist (BN303-30, Kempur Corp, China) and wet etching to ensure electric contact with the C-PDMS electrodes and form external-wiring pads. Oxygen plasma was used to enhance the adhesion of ITO glass and C-PDMS.

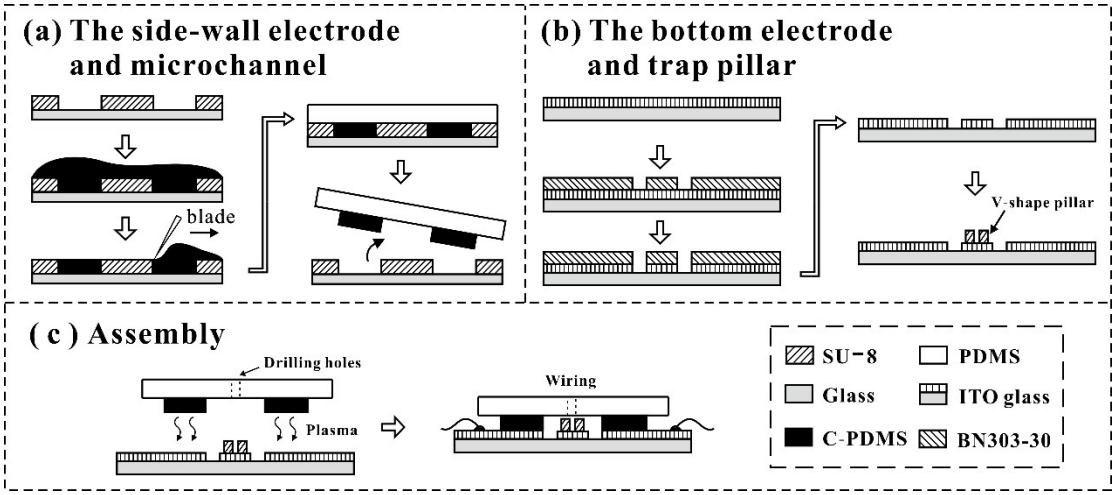

Figure S5 | The fabrication procedure for the micro-device. **(a)** The fabrication procedure for the sidewall electrodes and microchannel. **(b)** The fabrication procedure for the bottom electrode and trap pillars. (c) Assembly of the two parts.

Single-shell cell model

Fig. S6 shows the single-shell dielectric model for a cell and its equivalent homogeneous sphere model.

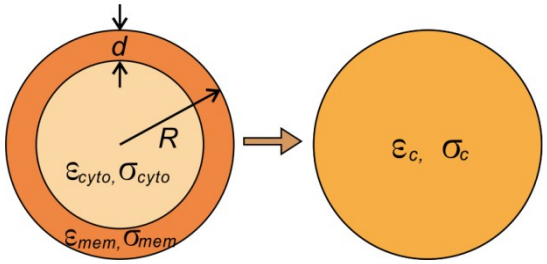

Fig. S6. The single-shell model of a cell and its equivalent homogeneous sphere model.

The effective complex permittivity of the equivalent homogeneous sphere can be expressed as

$$\varepsilon_c^* = \varepsilon_{mem}^* \frac{\left(\frac{R}{R-d}\right)^3 + 2\left(\frac{\varepsilon_{cyto}^* - \varepsilon_{mem}^*}{\varepsilon_{cyto}^* + 2\varepsilon_{mem}^*}\right)}{\left(\frac{R}{R-d}\right)^3 - \left(\frac{\varepsilon_{cyto}^* - \varepsilon_{mem}^*}{\varepsilon_{cyto}^* + 2\varepsilon_{mem}^*}\right)} \tag{S9}$$

$$\approx \varepsilon_{mem}^{*} \frac{\frac{r^3}{r^3 - 3r^2 d} + 2\left(\frac{\varepsilon_{cyto}^{*} - \varepsilon_{mem}^{*}}{\varepsilon_{cyto}^{*} + 2\varepsilon_{mem}^{*}}\right)}{\frac{r^3}{r^3 - 3r^2 d} - \left(\frac{\varepsilon_{cyto}^{*} - \varepsilon_{mem}^{*}}{\varepsilon_{cyto}^{*} + 2\varepsilon_{mem}^{*}}\right)}$$

$$\approx \frac{\frac{\varepsilon_{mem}^{*}}{d} R \cdot \varepsilon_{cyto}^{*}}{R \cdot \frac{\varepsilon_{mem}^{*}}{d} + \varepsilon_{cyto}^{*}}$$

$$= C_{mem}^{*} \frac{R \cdot \varepsilon_{cyto}^{*}}{R \cdot C_{mem}^{*} + \varepsilon_{cyto}^{*}},$$

where R and d are the outer radius and the membrane thickness of the single-shell dielectric model, respectively. $\varepsilon_{mem}^{*} = \varepsilon_{mem} - j\frac{\sigma_{mem}}{\omega}$, $\varepsilon_{cyto}^{*} = \varepsilon_{cyto} - j\frac{\sigma_{cyto}}{\omega}$, $C_{mem}^{*} = C_{mem} - j\frac{G_{mem}}{\omega}$, $C_{mem} = \frac{\varepsilon_{mem}}{d}$ is the area-specific membrane capacitance, and $G_{mem} = \frac{\sigma_{mem}}{d}$ is the area-specific membrane conductance.

The effects of four dielectric parameters of the cell on the rotation spectrum

Using Equations 2 and 8, we calculated the rotation speed for a given set of parameters, including the four dielectric parameters of the cell (ε_{mem}, σ_{mem}, ε_{cyto}, σ_{cyto}). The parameters were assigned with typical values adopted from literature and summarized in Table S1. We plot the rotation spectral curves with respect to each of these four parameters in Fig. S6.

The conductivity of cell membrane has negligible influence on the rotation spectrum at the full frequency range (Fig. S6a). The permittivity of cytoplasm has negligible effect on the rotation spectrum (Fig. S6d) when the frequency < 100 MHz. The permittivity of cell membrane and the conductivity of cytoplasm make significant difference to the rotation spectrum when the frequency < 100 MHz (Fig. S6bc), facilitating the spectrum-based measurement of these two parameters membrane permittivity. In normal laboratory setting, the AC signal generator has an upper frequency limit of 50 MHz like the one we used in the experiment. Hence, for the sake of experimental settings, the electrorotation-based method of extracting cell dielectric properties is inherently not able to differentiate the conductivity of cell membrane or the permittivity of cytoplasm. Therefore, in experiment, these two variables can be assigned a random value with no worry to affect the extraction of the other two variables.

Table. S1 The values assigned to cell and medium parameters in calculating the rotation spectrum.

	σ_{mem} (μS/m)	ε_{mem}	σ_{cyto} (S/m)	ε_{cyto}

Fig. S7a	**1~10**	$12\varepsilon_0$	0.4	$100\varepsilon_0$
Fig. S7b	10	**$1\sim20\varepsilon_0$**	0.4	$100\varepsilon_0$
Fig. S7c	10	$12\varepsilon_0$	**0.1~1**	$100\varepsilon_0$
Fig. S7d	10	$12\varepsilon_0$	0.4	**$10\sim100\varepsilon_0$**

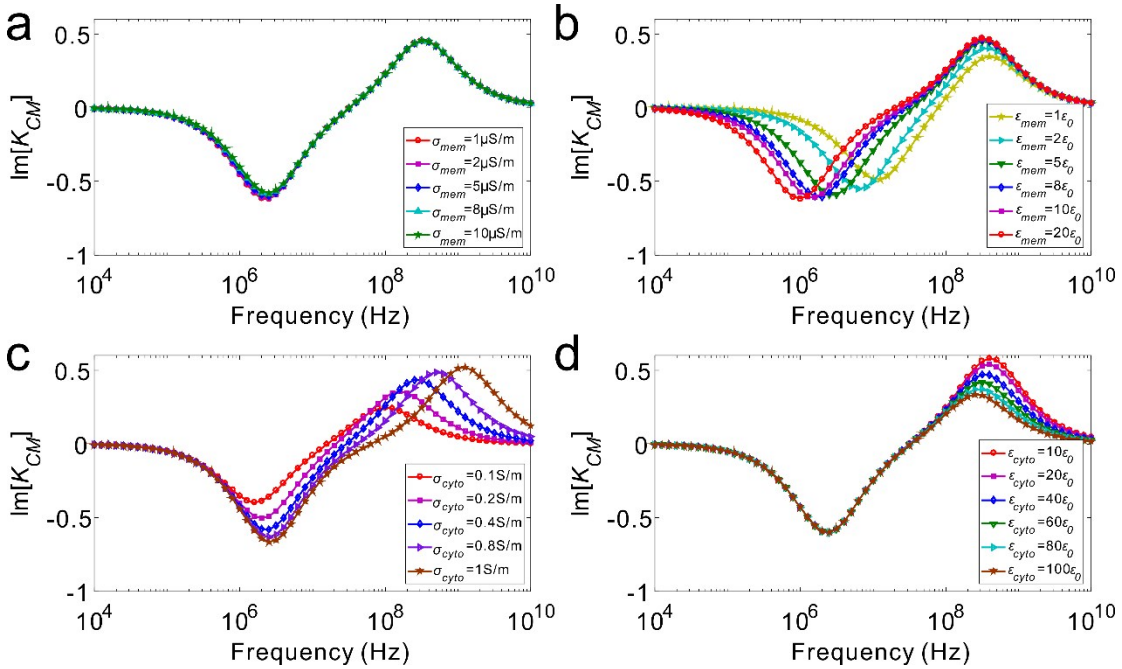

Fig. S7. The influence of four dielectric parameters of the cell on the rotation spectrum. **(a)** Conductivity of membrane. **(b)** Permittivity of membrane. **(c)** Conductivity of cytoplasm. **(d)** Permittivity of cytoplasm.

Notes

In the experiment, extra care was take to minimize the problems of cell lysis, Joule heating and water electrolysis, by selecting proper experimental conditions. (a) When the voltage applied in the experiment is large enough, the cell will lysis after touching the electrode. Because an excessively high electric field strength not only affects the permeability of the cell membrane, but also increases membrane voltage. Once the membrane voltage is greater than 1 V, electroporation will happen. (b) Excessive joule heating can affect cell viability and induce heat transmission of medium. Joule heating is positively correlated with AC signal amplitude and medium conductivity. In experiment, low-conductivity (36.5 mS/m) DEP buffer was used and the amplitude of the signal was confined below 14.5 V. (c) Water electrolysis occurs when the AC frequency is low or the voltage amplitude is high. To mitigate electrolysis, the AC signals were set in the range of 100 kHz~10 MHz and <14.5 V.